GPS Solutions (2023) 27:136
https://doi.org/10.1007/s10291-023-01477-7

ORIGINAL ARTICLE

Real-time multi-GNSS precise point positioning with ambiguity resolution based on the BDS-3 global short-message communication function

Ziyuan Song[1,2] · Junping Chen[1,2,3] · Yize Zhang[1,2] · Chao Yu[1,2] · Junsheng Ding[1,2]

Received: 16 September 2022 / Accepted: 22 May 2023

Abstract
Real-time precise point positioning (PPP) with ambiguity resolution (PPP-AR) has been realized with the provision of various precise correction parameters from IGS multi-GNSS experiment (MGEX) centers via the Internet and commercial services via communication satellites. For users in remote regions with no access to the Internet, e.g., oceans and deserts, BDS-3 provides an open and free prototype for global users to receive precise positioning services through its global short-message communication (GSMC) function. However, limited by the bandwidth and parameter update frequency, the set of precise correction parameters from MGEX or other resources cannot be fully transmitted to users. To address this issue and improve the positioning performance of the BDS GSMC service, we propose a real-time multi-GNSS PPP-AR method based on real-time state space representation (SSR) corrections, where a novel strategy for the generation, encoding and broadcast of the correction parameters is developed. The new model maintains the accuracy of the correction parameters to the largest extent while meeting the interface requirement of BDS GSMC regarding the bandwidth and parameter update frequency. Experiments show that the new strategy effectively improves positioning performance compared to conventional GSMC-based float-ambiguity PPP. Specifically, in a kinematic experiment, the positioning precision improved by 10%, and the convergence time was shortened by 15%, with an average 71% successfully fixed rate. Beyond that, with the proposed extrapolatable corrections, the validity time of corrections is significantly prolonged from 2.5 to 7.5 min when a centimeter-level accuracy is needed. Thus, the continuity of the positioning service is guaranteed even if an unexpected short-term interruption occurs in the GSMC.

Keywords BDS-3 · Global short-message communication · Real-time PPP-AR · Correction encoding · Correction broadcast

Introduction

Precise point positioning (PPP) has significantly progressed over the last two decades (Malys and Jensen 1990; Zumberge et al. 1997; Kouba and Héroux 2001). Scholars have studied real-time PPP since 2013 (Chen et al. 2013), when the open-access real-time service (RTS) was officially launched by the International GNSS Service (IGS). Based on the broadcast ephemeris, the real-time orbit, clock and other corrections are provided to users (IGS 2020). The corrections are formatted into state space representation (SSR) messages and transmitted to users based on the Radio Technical Commission for Maritime Services (RTCM) standard (RTCM 2016) via the Internet according to the Networked Transport of RTCM via Internet Protocol (NTRIP) (Weber et al. 2007). Since then, RTS PPP has been widely used and proved to satisfy decimeter-to-centimeter accuracy (Shi et al. 2017; Wang et al. 2022).

The long convergence time attributed to the float ambiguities that absorb the hardware phase delay has been an inherent weakness for PPP (Geng et al. 2010). Hence, the PPP ambiguity resolution (PPP-AR) method has been proposed

✉ Junping Chen
junping@shao.ac.cn

1 Shanghai Astronomical Observatory, Chinese Academy of Sciences, Shanghai 200030, China

2 School of Astronomy and Space Science, University of Chinese Academy of Sciences, Beijing 100049, China

3 Shanghai Key Laboratory of Space Navigation and Positioning Techniques, Shanghai 200030, China

Published online: 04 June 2023

and widely researched. The uncalibrated phase bias (UPD) method (Ge et al. 2008), along with the integer clock method (Geng et al. 2012), have become the major solutions for PPP ambiguity resolution. To implement RTS for PPP-AR, several multi-GNSS experiment (MGEX) centers provide products. For instance, based on the UPD method, the Centre National d'Etudes Spatiales (CNES) started to broadcast observation-specific UPD corrections in 2019, while Wuhan University (WHU) broadcasts their calibrated clock products along with the wide-lane integer ambiguity according to the integer clock method. The product precision of several analysis centers are compared with each other and the service of CNES is currently the most stable with the highest accuracy (Li et al. 2022). Meanwhile, multi-GNSS real-time PPP-AR methods have been developed in quick succession, and their superior performance to float-ambiguity PPP has been proved (Liu et al. 2020; Chen et al. 2021). Although the RTS for PPP-AR significantly expands its scenes to be used, the network transmission is still an obstacle to users situated in special geographical areas, such as the desert and ocean, where Internet and RTK service are unavailable.

The short-message communication (SMC) service, as a feature of the BeiDou Satellite Navigation system (BDS), supports two-way communications between the user and server. Signal transmission is based on BDS satellites, which removes the limitation of the distance between the user and server (Li et al. 2021; Chen et al. 2022a). Based on the unique advantage of the BDS SMC service, RTS corrections can be broadcast to users. Nevertheless, the capacity of the BDS SMC service is the largest barrier for broadcasting SSR corrections. For BDS-2 regional SMC (RSMC), 628 bits at most are available for civilian users (CSNO 2015), and for BDS-3 global SMC, the number of bits is limited to 560 (CSNO 2019). The minimum communication frequency is limited to 1 min (Yang et al. 2019). However, in actual situation, constrained by user priority and satellite bandwidth, the communication frequency of SMC can be prolonged to 2–3 min, sometimes even more than 5 min. In addition, considering the system response delay, along with the transmission time span, the service delay for the user may up to 2 s (CSNO 2021). Therefore, the minimum interval for the user to receive information through BDS SMC is about 62 s. In contrast, the minimum bandwidth for one epoch of SSR corrections in RTCM is 6628 bits (Nie et al. 2020), and for most MGEX centers, the broadcast frequency is set to 5 s. Thus, many scholars have devoted attention to implementing real-time PPP using BDS SMC. Li et al. (2019) used multiple sets of BDS-2 RSMC devices to broadcast land-based reference observations for offshore relative positioning. Nie et al. (2020) proposed an offshore real-time precise point positioning technique based on a single set of BDS-2 RSMC devices to reduce the amount of equipment further. The SSR corrections are simplified to user-range equivalent corrections, and the range corrections are broadcast to users along with their rate. Geng et al. (2022) and Gu et al. (2022) implement RTS PPP using BDS-3 GSMC, and different encoding strategies are proposed in their studies.

In the research mentioned above, the implementation of multi-GNSS PPP-AR via BDS GSMC has not been studied. The UPD, an indispensable correction for ambiguity resolution, has to be transmitted to the user, which brings new challenges due to the limited GSMC bandwidth. To further optimize the positioning performance and reduce the convergence time for GSMC-based PPP, we present a new method to implement real-time multi-GNSS PPP-AR using GSMC.

In "Methodology" section, the overall system composition is introduced at first. Then, the method of SMC-suited correction generation, fitting, encoding and broadcasting strategies for servers is proposed. In addition, the SMC-based PPP-AR implementation method using those corrections is introduced. In "Experiments and analysis" section, the optimal options for fitting the corrections described in "Methodology" section are further analyzed, followed by the evaluation of the SMC-based PPP-AR performance. Moreover, the performance of BDS SMC transmission and its influence on positioning are analyzed. The conclusions are summarized in "Conclusions" section.

Methodology

In most existing GSMC-based PPP research, only orbit and clock corrections are considered to be transmitted, and float-ambiguity PPP is conducted on the user end. In this study, to implement PPP-AR via GSMC, the UPD is broadcast to users, which brings challenges due to the limited bandwidth. Thus, a new correction generation, encoding and broadcasting method suitable for SMC-based PPP-AR is proposed in this section.

Overall system composition

As shown in Fig. 1, the system is composed of three parts, including an external real-time SSR provider, a server end and the user end. Real-time SSR products can be retrieved from IGS RTS or a commercial company via a server on the Internet at an interval of seconds. Nonetheless, considering the bandwidth and frequency limitation of BDS-3 GSMC, the corrections cannot be directly transmitted to users via BDS-3 GSMC.

To address this issue, the server first obtains the user's approximate coordinate using the two-way communication function of BDS-3 GSMC. Then, the orbit and clock corrections can be converted to observation space representation (OSR) corrections, which effectively saves GSMC

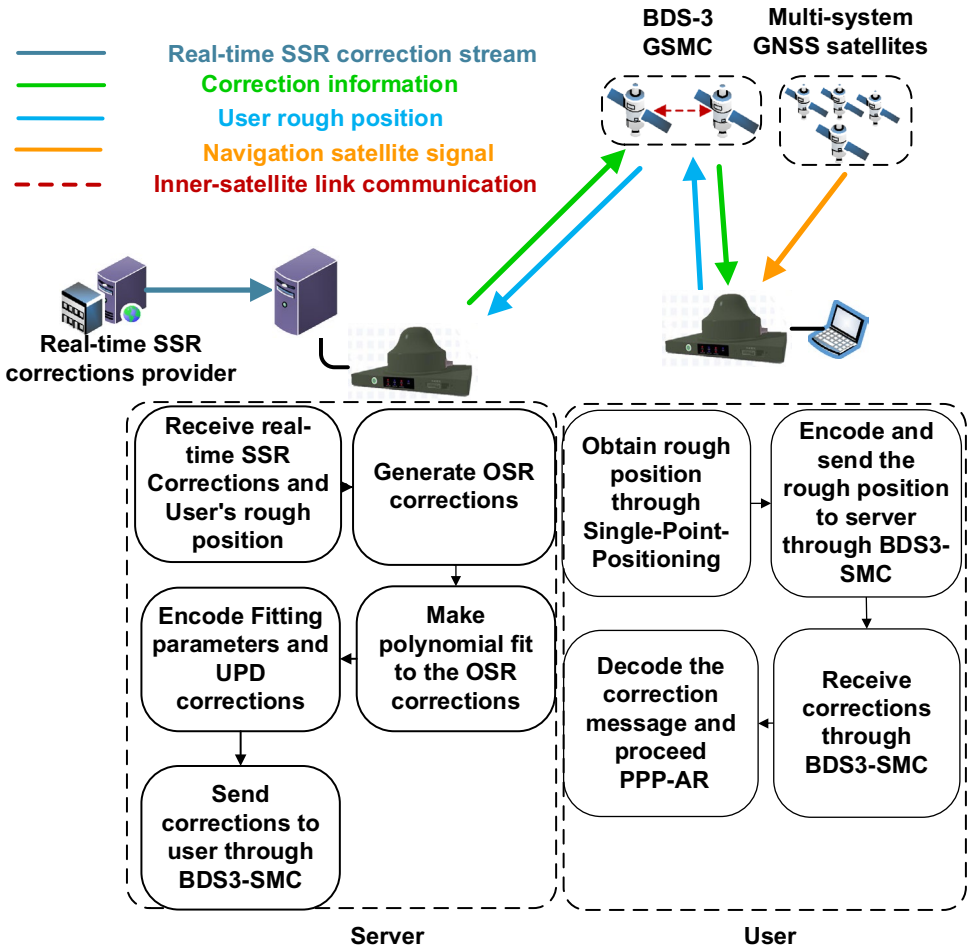

Fig. 1 BDS-3 GSMC-based PPP-AR system composition and processing flow diagram. Based on a real-time SSR stream, corrections are generated, encoded and broadcast by the server (bottom left flowchart). The user (bottom right flowchart) conducts real-time PPP-AR using the corrections transmitted via BDS-3 GSMC

bandwidth. The specific method is introduced in "OSR correction generation method" section.

However, it is still barely possible to transmit the complete corrections of the multisystem to users in one epoch since the UPDs are also indispensable for PPP-AR, which occupy a large proportion of the bandwidth. Therefore, regarding the OSR correction as the parameter with short-term variability, its trend characteristic is analyzed and fitted with polynomial coefficients. In addition, ignoring the time-varying error, the UPD on each frequency is regarded as a constant over a few minutes (Geng et al. 2010). The coefficients and UPDs are encoded reasonably based on their range distribution and accuracy requirements. Since the PRN list of satellites visible to the user is available, the encoded corrections of all satellites are sent in batches from the server within 2–3 min with 1-min intervals via GSMC.

After receiving and decoding the corrections, users may use the polynomial coefficients to extrapolate the OSR corrections to the current time and correct the satellite phase biases using the UPDs. Therefore, multi-GNSS real-time PPP-AR can be implemented in a few minutes when the corrections for different systems are received.

OSR correction generation method

SSR corrections are first transformed into OSR corrections at the server to compress the data volume since the user's rough position has been obtained via GSMC. The real-time SSR orbit corrections are composed of radial, along-track and cross-track direction corrections $(\delta_r^s, \delta_a^s, \delta_c^s)$ and their first-order derivative $\left(\dot{\delta}_r^s, \dot{\delta}_a^s, \dot{\delta}_c^s\right)$. The satellite corrections δ^s in the satellite coordinate system are expressed as:

$$\delta^s = \begin{bmatrix} \delta_r^s \\ \delta_a^s \\ \delta_c^s \end{bmatrix} + \begin{bmatrix} \dot{\delta}_r^s \\ \dot{\delta}_a^s \\ \dot{\delta}_c^s \end{bmatrix} \times \left(t - t_0\right) \tag{1}$$

where t and t_0 denote the current time and the SSR epoch time, respectively.

The real-time SSR clock corrections are composed of the polynomial coefficients C_0, C_1 and C_2. The clock correction δC^s at the current time is expressed as:

$$\delta C^s = C_0 + C_1 \times \left(t - t_0\right) + C_2 \times \left(t - t_0\right)^2 \tag{2}$$

To transform the orbit corrections from the satellite coordinate system to the Earth-centered Earth-fixed (ECEF) frame, the conversion formula is:

$$\delta X^s = \left[\boldsymbol{e}_r, \boldsymbol{e}_a, \boldsymbol{e}_c\right] \cdot \delta^s \tag{3}$$

$$\text{with} \quad \begin{cases} \boldsymbol{e}_r = \boldsymbol{e}_a \times \boldsymbol{e}_c \\ \boldsymbol{e}_c = \frac{\boldsymbol{r} \times \dot{\boldsymbol{r}}}{|\boldsymbol{r} \times \dot{\boldsymbol{r}}|} \\ \boldsymbol{e}_a = \frac{\dot{\boldsymbol{r}}}{|\dot{\boldsymbol{r}}|} \end{cases} \tag{4}$$

where δX^s denotes the orbit corrections in the ECEF frame and $\boldsymbol{r}$ and $\dot{\boldsymbol{r}}$ represent the position and velocity vectors of the satellites in the ECEF frame, which can be calculated using the broadcast ephemeris.

The OSR correction $\delta \mathrm{OSR}^s$ can be expressed as:

$$\delta \mathrm{OSR}^s = c \cdot \delta C^s - \boldsymbol{e} \cdot \delta X^s \tag{5}$$

$$\text{with} \quad \boldsymbol{e} = \frac{\boldsymbol{P}^s - \boldsymbol{P}_r}{\left|\boldsymbol{P}^s - \boldsymbol{P}_r\right|} \tag{6}$$

where $\boldsymbol{e}$ denotes the direction vector from user station to the satellite and c represents the light speed. $\boldsymbol{P}^s$ and $\boldsymbol{P}_r$ denote the vector for satellite and receiver in ECEF frame, respectively.

The implementation of OSR corrections efficiently reduces the data volume. Furthermore, the strategy is more consistent with the BDS broadcast ephemeris, as the BDS employs a dedicated ephemeris refinement strategy to maintain the minimum signal-in-space range error (SISRE), which is also an OSR-based strategy (Chen et al. 2022b).

OSR correction fitting method

Using the methods in Geng et al. (2022) and Gu et al. (2022), the OSR corrections in previous section are encoded and directly broadcast to users. When unexpected communication interruption occurs in GSMC, the accuracy of OSR corrections deteriorates rapidly with increasing interruption duration. Therefore, to extend the validity time for OSR corrections, we apply a polynomial fitting to them using the latest continuous data. Although it is mentioned in Nie et al. (2020), the rate of corrections is broadcast to users, and the characteristic of the corrections and optimal fitting strategy is not analyzed in detail.

To determine the appropriate fitting order, the short-term change tendency is determined in advance. The SSR corrections from CNES are used for OSR conversion, and Fig. 2 shows the time series of OSR corrections for certain satellites on each system. The change shows a linear trend in the short term. Beyond that, a correction jump occurs for each satellite with broadcast ephemeris updates. However, for BDS satellites in particular, an extra value jump is noticed in addition to the broadcast ephemeris change.

To highlight this jump bias, additional BDS satellite OSR correction time series are shown in Fig. 3. The non-ephemeris-switch jump shows consistency for all BDS satellites. To verify the cause of this jump, we use the final clock product from IGS to be compared with the CNES real-time clock.

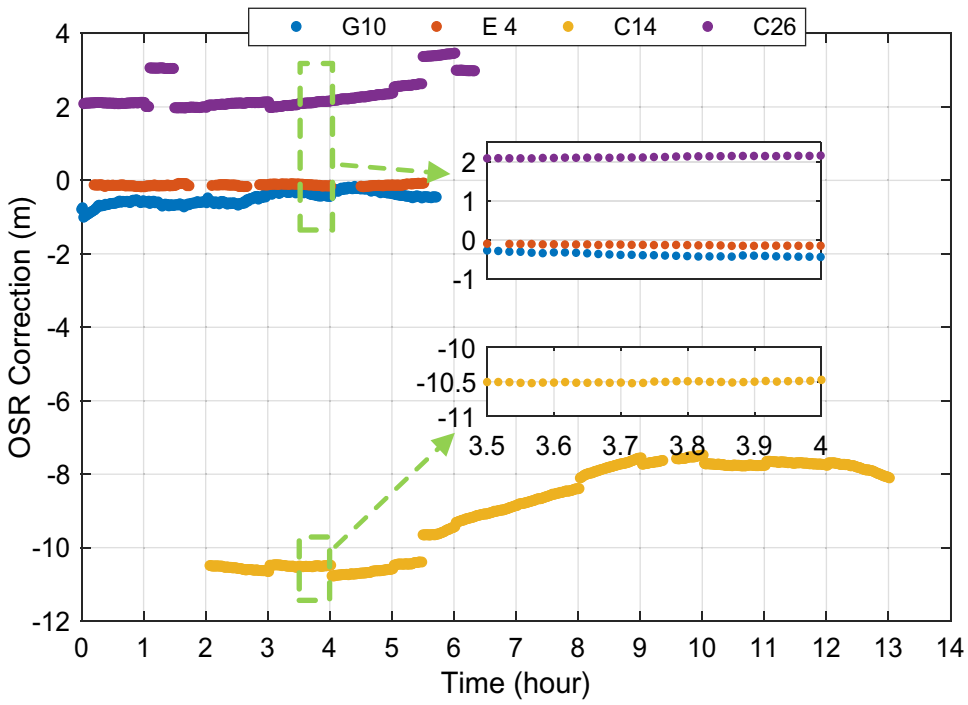

Fig. 2 OSR correction time series for G10, E04, C14 and C26. Station: KOUR, DOY 192 (2022)

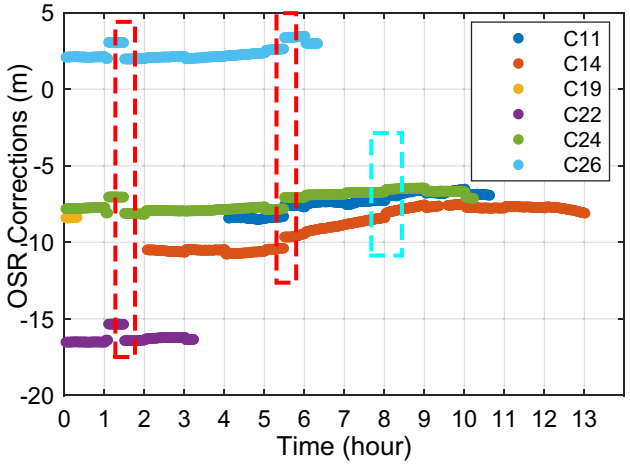

Fig. 3 OSR correction time series for several BDS satellites. Station: KOUR, DOY 192 (2022). Note that the ephemeris-switch jump occurs right after the change of the whole hour. As shown in the blue box, the jump biases are different for each satellite. The red boxes indicate the overall OSR jumps at non-ephemeris-switch moments. For all BDS satellites, the jump biases are consistent

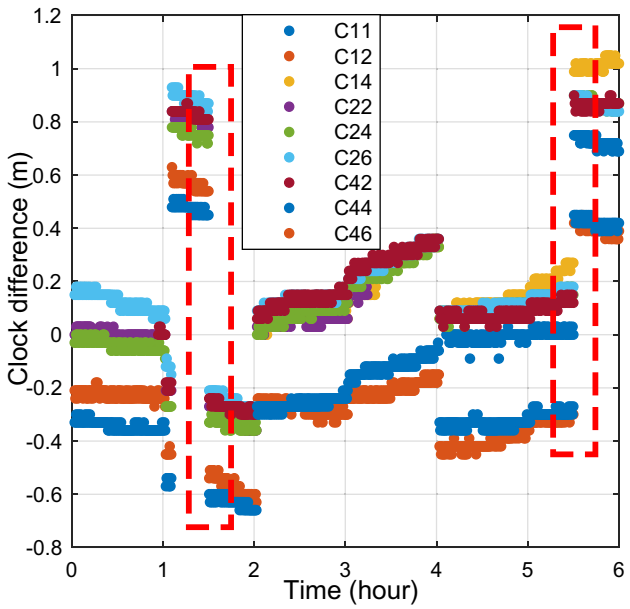

Fig. 4 Differenced clock time series between CNES real-time product and IGS final product for BDS satellites. DOY 192 (2022). The red box indicates that compared to the IGS final clock product, CNES real-time clock has extra overall jumps for BDS satellites besides the ephemeris-switch jump

After deducting the system deviation of IGS final clock product and CNES real-time clock product, we make the difference between two clock series. Figure 4 shows some BDS satellite clock series after difference. The red box indicates the overall clock jump for BDS satellites using CNES real-time clock at non-ephemeris-switch moment, and the jump moments are consistent with the OSR jumps shown in Fig. 3. Therefore, we attribute the non-ephemeris-switch jump of BDS OSR to the CNES clock products. We did the same experiments for GPS and Galileo, and the jump was not appeared in their real-time clock products.

Considering the linear tread of the OSR time series, linear polynomial fitting is applied to fit the OSR corrections, and the fitting formula is expressed as:

$$\begin{bmatrix} \delta\mathrm{OSR}^s_{t_1} \\ \vdots \\ \delta\mathrm{OSR}^s_{t_i} \\ \vdots \\ \delta\mathrm{OSR}^s_{t_n} \end{bmatrix} = \begin{bmatrix} 1 \\ \vdots \\ 1 \\ \vdots \\ 1 \end{bmatrix} \cdot a_0^{\mathrm{OSR}} + \begin{bmatrix} t_1 - t_1 \\ \vdots \\ t_i - t_1 \\ \vdots \\ t_n - t_1 \end{bmatrix} \cdot a_1^{\mathrm{OSR}} \tag{7}$$

where $\delta\mathrm{OSR}^s_{t_i}$ denotes the OSR correction of satellite s at time t_i; a_0^{OSR} and a_1^{OSR} represent the constant term and linear term coefficients of $\delta\mathrm{OSR}^s$ at time t_n, respectively; and t_n denotes the latest time of corrections.

To eliminate the value jump caused by the broadcast ephemeris switch while fitting, the OSR correction with the new IODE needs to make the following conversion:

$$\delta\mathrm{OSR}^s = \mathrm{Coor}_f - \left(\mathrm{Coor}_c - \delta\mathrm{OSR}^{s'}\right) \tag{8}$$

where Coor_f refers to the satellite coordinates calculated with the broadcast ephemeris before switching; Coor_c refers to the satellite coordinates calculated with the current broadcast ephemeris after switching; and $\delta\mathrm{OSR}^{s'}$ and $\delta\mathrm{OSR}^s$ represent the OSR corrections after and before ephemeris switching, respectively. This conversion is used until the IODE of all fitting data change to the most recent.

To maintain the continuity of parameter fitting through BDS satellite OSR correction jumps, correction alignment is necessary for the OSR corrections with time labels prior to the jump epoch, which can be expressed as:

$$\delta\mathrm{OSR}^s_{\mathrm{BDS}} = \delta\mathrm{OSR}^{s'}_{\mathrm{BDS}} + d\mathrm{OSR}^s_{\mathrm{BDS}} \tag{9}$$

where $d\mathrm{OSR}^s_{\mathrm{BDS}}$ denotes the jump variation of the OSR correction on satellite; and $\delta\mathrm{OSR}^{s'}_{\mathrm{OSR}}$ and $\delta\mathrm{OSR}^s_{\mathrm{BDS}}$ denote the OSR correction used for fitting on satellite before and after the switch, respectively.

To further optimize the linear fitting strategy, the fitting accuracies, along with the optimal number of fitted samples, are analyzed in "Experiments and analysis" section.

OSR correction encoding strategy

In this research, the GPS, Galileo and BDS systems are used to implement multi-GNSS ionosphere-free PPP-AR and the largest obstacle is the limitation of bandwidth. To economize the GSMC bits, code bias can be omitted by using L1/L2 for GPS, E1/E5a for Galileo and B1I/B3I for BDS. In addition,

the indispensable corrections, including a_0^{OSR}, a_1^{OSR} and the UPDs, on both frequencies of each system, need further simplification during encoding.

Geng et al. (2022) analyzed the range attribution of the user-range equivalent correction. In this research, the sort and amount of the corrections are distinct. To determine the range of the corrections, one week of corrections and their range distributions were analyzed statistically. As shown in Fig. 5, the corrections for GPS and Galileo are centrally distributed, as their a_0^{OSR} is within ±2 m, their a_1^{OSR} is within ±1 mm/s and most UPD corrections are within ±2 m. In contrast, those for BDS are quite discrete. Since the BDS clock in broadcast ephemeris is based on B3I (Chen et al. 2020, 2022c), while the SSR is based on B1I/B3I, a distinct deviation exists for BDS corrections (Geng et al. 2022). Beyond that, the poor orbit and clock accuracy of BDS-2 also contributes to the large value of corrections. Note that the datum bias of BDS correction can be eliminated at the server using broadcast ephemeris timing group delays (TGDs) to reduce the range (Zhang et al. 2020). The comparison of the range before and after eliminating the datum bias for BDS is shown in blue and red in Fig. 5, respectively. It can be verified that after datum conversion, most a_0^{OSR} corrections are within ±3 m. Owing to the limitation of GSMC capacity, satellites with large value corrections cannot be encoded.

Apart from the corrections, the time information and the number of satellites in each epoch are also indispensable to users. We use GPS time to mark the epoch time. To compress the space of the header part, the simplified GPS week is broadcast instead of the original GPS week. The conversion is expressed as:

$$\mathrm{Week}_s = \mathrm{Week}_c - 2000 \tag{10}$$

where Week_s and Week_o refer to the simplified GPS week and complete GPS week, respectively. The header part encoding strategies are shown in Table 1.

Considering that the real-time SSR orbit correction accuracy on the radial plane is more than 2 cm and the clock correction accuracy is more than 0.1 ns (Li et al. 2022), and 0.1 cycles of the carrier phase are approximately 2 cm, encoding

Table 1 Header part encoding strategies of BDS-3 GSMC correction information

Header part	Range	Value accuracy	Effective range (decimal)	Size
Simplified GPS week	1 ~ 1024	1	1 ~ 1024	10 bits
GPS second	0 ~ 604,800	1	0 ~ 604,800	20 bits
Number of satellites	4	1	0 ~ 10	4 bits
Total	–			34 bits

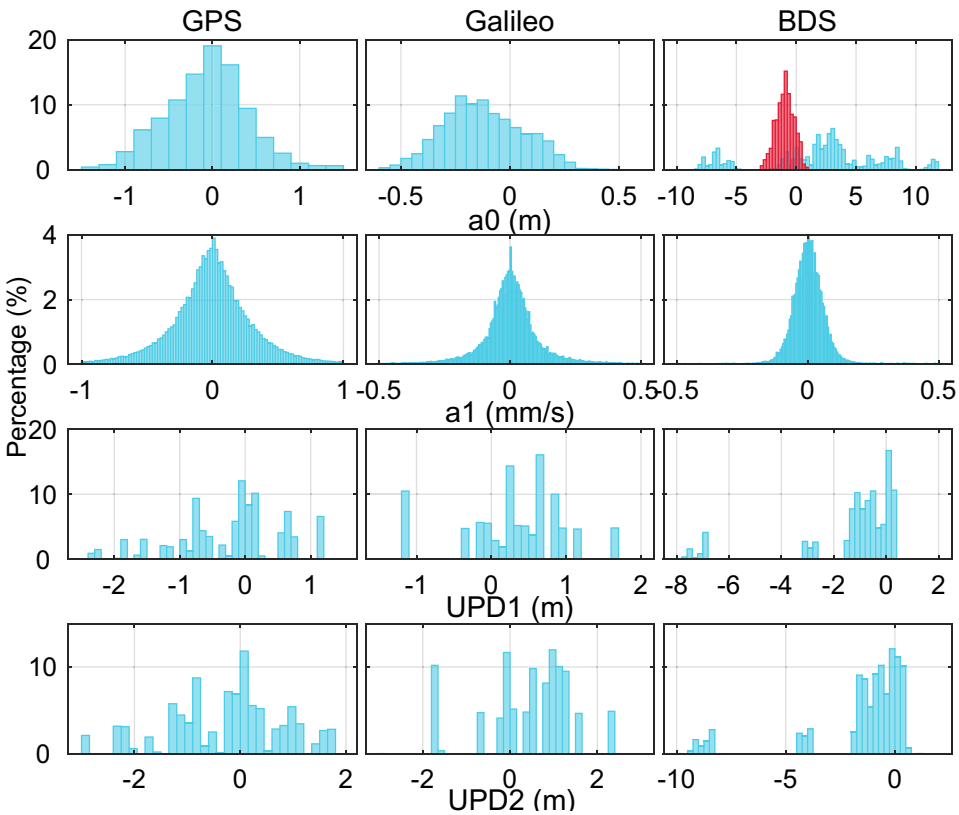

Fig. 5 Percentage distribution of a_0^{OSR}, a_1^{OSR} and the UPD on each frequency. Data of GPS, Galileo and BDS system are displayed in each column. For the a_0^{OSR} of the BDS, its distribution after the change of datum is particularly marked with the red bars

Table 2 Encoding strategies for each BDS-3 GSMC satellite correction information

Body part	Range	Value accuracy	Effective range (decimal)	Size
System	0 ~ 2	1	0 ~ 2	2 bits
PRN	1 ~ 63	1	1 ~ 63	6 bits
IODE	0 ~ 255	1	0 ~ 255	8 bits
a_0	± 3 m	6 mm	0 ~ 1000	10 bits
a_1	±1 mm/s	0.125 mm/s	0 ~ 15	4 bits
UPD_1	± 2 m	8 mm	1 ~ 500	9 bits
UPD_2	±2 m	8 mm	1 ~ 500	9 bits
Total	–			48 bits

strategies are designed as shown in Table 2. In addition to the corrections, the system mark, PRN and IODE of satellites are encoded synchronously.

In each satellite correction, 48 bits of the bandwidth are occupied. Apart from the header part and the cyclic redundancy check (CRC) code at the end, ten satellite corrections can be broadcast to users via GSMC at one time. The whole message structure for one epoch is designed and shown in Fig. 6, where 546 bits are used, reserving 14 bits.

OSR correction broadcast and usage

As designed in the previous section, 10 satellite corrections at most can be broadcast to the user via GSMC simultaneously. However, the number of visible satellites may exceed 20 for a user tracking GPS, Galileo and BDS satellites. Using the linear fit coefficient OSR corrections designed in this research, we propose a correction broadcasting strategy in which all satellites visible to the user are taken into account.

To confirm the broadcast list of satellites, the satellite elevation threshold is set to 15°. In addition, the range of corrections must meet the requirement of the encoding strategy proposed in the previous section. For instance, we set the number of satellites to 30 and the communication frequency to 1 min, which will take about 2 min for the server to broadcast all the corrections. In this case, all satellites are divided into three groups, with 10 satellites in each group. Then, the corrections of each group are broadcast in sequence by the server, as shown in Fig. 7. The number of visible satellites and their OSR corrections may be different from 30, and the number of satellites in the final group may be less than 10. In this case, a few satellites from the first group are encoded in the latter to fulfill the 10-satellite-group completion. For real-time service, the above scheme loops to update the OSR correction of each satellite in a timely manner.

When the user receives corrections of the first group at the first epoch, the PPP-AR based on the 10 satellites is implemented. At the second epoch, corrections of the second group are received, and they are used along with the corrections of the first epoch. In the PPP-AR, observations of the 20 satellites can be used with the OSR corrections of the first group extrapolated. At the third epoch, corrections of the third group are received, and the PPP-AR is implemented using the complete 30 satellites, where OSR corrections of the first two groups are extrapolated. In the above scheme, the OSR correction of each satellite is refreshed when it is updated in the broadcast message.

BDS-3 GSMC-based PPP-AR for users

The ionospheric-free (IF) combination applied to the GSMC-based PPP-AR is expressed as:

$$\begin{cases} P^s_{\mathrm{IF},r} = \rho^s_r + c\cdot(\mathrm{d}t_r - dt^s) + M^s_r d_{\mathrm{trop},r} + (B_{\mathrm{IF},r} - B^s_{\mathrm{IF}}) - \delta\mathrm{OSR}^s + \varepsilon\left(P^s_{\mathrm{IF},r}\right) \\ \Phi^s_{\mathrm{IF},r} = \rho^s_r + c\cdot(\mathrm{d}t_r - \mathrm{d}t^s) + M^s_r d_{\mathrm{trop},r} - (b_{\mathrm{IF},r} - b^s_{\mathrm{IF}}) + \lambda_{\mathrm{IF}} N^s_{\mathrm{IF}} - \delta\mathrm{OSR}^s + \varepsilon\left(\Phi^s_{\mathrm{IF},r}\right) \end{cases} \tag{11}$$

where $P^s_{\mathrm{IF},r}$ and $\Phi^s_{\mathrm{IF},r}$ denote the IF combination of the pseudorange and carrier phase observations, respectively; ρ^s_r represents the geometrical propagation distances between satellite and receiver; $\mathrm{d}t_r$ and $\mathrm{d}t^s$ denote the receiver and satellite

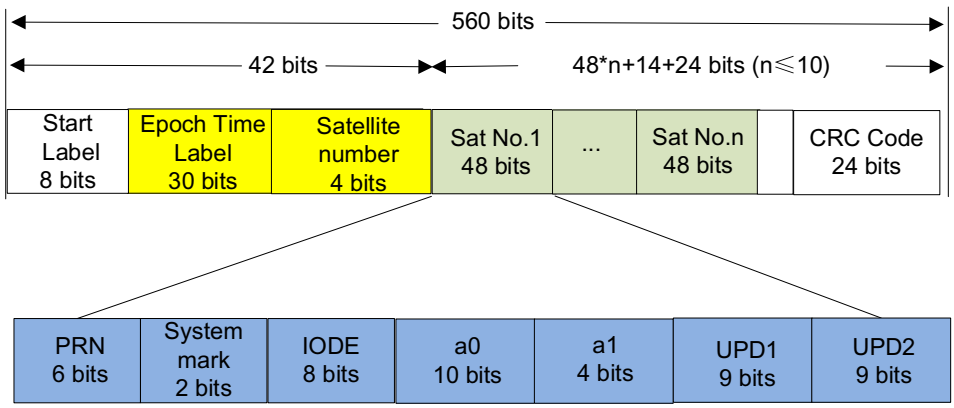

Fig. 6 Encoded BDS-3 GSMC correction structure for one epoch. The length of total message is 560 bits. The start label marks the starting point for decoding. The yellow panels represent the header. The green panels represent the body part, which may hold correction information for ten satellites for maximum capacity. The blue panels represent the encoded information for one satellite. The CRC Code is used for information correctness check

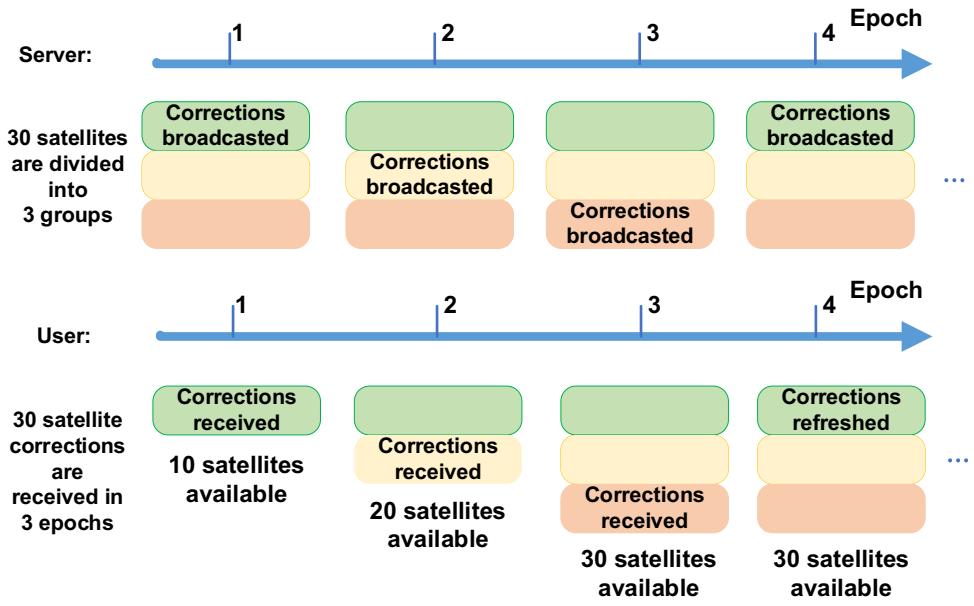

Fig. 7 Diagram of corrections broadcasting from the server and user use with 30 satellites as an example, where corrections of 10 satellites at maximum can be broadcast by GSMC in each epoch. The corrections of the 30 satellites are defined as 3 groups and broadcast in sequence; thus, it takes 3 epochs (about 3 min for the fastest) to accomplish the correction broadcasting of the 30 satellites. At the user end, OSR corrections are a combination of mixed-period extrapolation

clock error, respectively; $d_{\mathrm{trop},r}$ and M_r^s represent the wet zenith tropospheric delay and its mapping function, respectively; $B_{\mathrm{IF},r}$ and B_{IF}^s denote the code bias for the receiver and satellite, respectively; and $b_{\mathrm{IF},r}$ and b_{IF}^s represent the phase bias for the receiver and satellites, respectively. N_{IF}^s and λ_{IF} denote the IF phase ambiguity and its wavelength, respectively. $\varepsilon\left(P_{\mathrm{IF},r}^s\right)$ and $\varepsilon\left(\Phi_{\mathrm{IF},r}^s\right)$ represent the noise of the IF combination for pseudorange and carrier phase observations, respectively. Note that for BDS, the TGD corrections from B3I to B1I/B3I need to be considered additionally since the datum of BDS OSR corrections has been changed as mentioned in "Correction encoding strategy" section.

In (11), $\delta\mathrm{OSR}^s$ denotes the user-to-satellite direction error caused by the orbit and clock, which is calculated using the a_0^{OSR} and a_1^{OSR} received via BDS-3 GSMC and expressed as:

$$\delta\mathrm{OSR}^s = a_0^{\mathrm{OSR}} + a_1^{\mathrm{OSR}} \times \left(t - t_0\right) \tag{12}$$

As mentioned in the "Correction encoding strategy" section, B_{IF}^s is set to 0. b_{IF}^s is corrected by the UPD received from the server via GSMC since its short-term change error is neglected. $B_{\mathrm{IF},r}$ and $b_{\mathrm{IF},r}$ can be eliminated with between-satellite single-difference observations, which are expressed as:

$$\begin{cases} \nabla P_{\mathrm{IF},r}^s = \rho_r^s + c \cdot \left(\nabla \mathrm{d}t_r - \nabla \mathrm{d}t^s\right) + \nabla M_r^s d_{\mathrm{trop},r} - \nabla\delta\mathrm{OSR}^s + \varepsilon\left(P_{\mathrm{IF},r}^s\right) \\ \nabla \Phi_{\mathrm{IF},r}^s = \nabla\rho_r^s + c \cdot (\nabla \mathrm{d}t_r - \nabla \mathrm{d}t^s) + \nabla M_r^s d_{\mathrm{trop},r} - b_{\mathrm{IF}}^s + \lambda_{\mathrm{IF}} \nabla N_{\mathrm{IF}}^s - \nabla\delta\mathrm{OSR}^s + \varepsilon\left(\Phi_{\mathrm{IF},r}^s\right) \end{cases} \tag{13}$$

where ∇ represents the between-satellite single difference of variables. Then, ∇N_{IF}^s can be estimated with a Kalman filter (Zumberge et al. 1997), in which the code and phase biases have been eliminated.

To address the narrow-lane ambiguity ∇N_{NI}^s, the integer wide-lane ambiguity N_{WL}^s first needs to be fixed (Ge et al. 2008). N_{WL}^s can be expressed as:

$$\tilde{N}_{\mathrm{WI}}^s = N_{\mathrm{WI}}^s + \mathrm{UPD}_{\mathrm{WI},r} - \mathrm{UPD}_{\mathrm{WI}}^s \tag{14}$$

where $\tilde{N}_{\mathrm{WI}}^s$ represents the float wide-lane ambiguity and $\mathrm{UPD}_{\mathrm{WI}}^s$ and $\mathrm{UPD}_{\mathrm{WI},r}$ represent the wide-lane UPD on the satellite and receiver, respectively. It must be noted that for the $\mathrm{UPD}_{\mathrm{WI}}^s$ corrections sent from CNES, the satellite and receiver phase center offset (PCO) has been deducted; thus, those for the wide-lane ambiguity N_{WI}^s must be subtracted as well (Geng et al. 2021), which is expressed as:

$$N_{\mathrm{WI}}^s = \lambda_{\mathrm{WI}}\left(\frac{\Phi_{1,r}^s + z_{1,r}^s}{\lambda_1} - \frac{\Phi_{2,r}^s + z_{2,r}^s}{\lambda_2}\right) - \frac{f_1\left(P_{1,r}^s + z_{1,r}^s\right) + f_2\left(P_{2,r}^s + z_{2,r}^s\right)}{f_1 + f_2} \tag{15}$$

$$\text{with} \begin{cases} z_{1,r}^s = z_{1,r} \sin\theta_r^s + z_1^s \\ z_{2,r}^s = z_{2,r} \sin\theta_r^s + z_2^s \end{cases} \tag{16}$$

where λ denotes the wavelength; Φ denotes the carrier phase observations; P denotes the pseudorange observations; f

denotes the frequency; $z_{i,r}$ denotes the vertical phase center offsets of the receiver antenna on frequencies i; similarly, z_i^s are those for the satellite antenna; and θ_r^s denotes the elevation angle of satellite s with respect to receiver r.

Similar to the IF ambiguity, $\mathrm{UPD}_{\mathrm{Wl}}^s$ can be corrected with GSMC corrections. $\mathrm{UPD}_{\mathrm{Wl},r}$ can be eliminated with between-satellite single-difference observations. Afterward, the between-satellite single-difference wide-lane ambiguity ∇N_{Wl}^s is rounded off to an integer for fixing.

The between-satellite single-difference narrow-lane ambiguity can be expressed as:

$$\nabla \tilde{N}_{\mathrm{Nl}}^s = \nabla \tilde{N}_{\mathrm{IF}}^s - \nabla N_{\mathrm{Wl}}^s \tag{17}$$

where $\nabla \tilde{N}_{\mathrm{Nl}}^s$ and $\nabla \tilde{N}_{\mathrm{IF}}^s$ represent the between-satellite single-difference float narrow-lane ambiguity and float IF ambiguity, respectively. ∇N_{WL}^s represents the fixed between-satellite single-difference wide-lane ambiguity.

Since $\nabla \tilde{N}_{\mathrm{IF}}^s$ has been estimated in (13) and ∇N_{WL}^s has been fixed in (14), $\nabla \tilde{N}_{\mathrm{Nl}}^s$ can be calculated, and furthermore, the LAMBDA (Teunissen 1995; Li et al. 2013) is applied to fix the narrow-lane ambiguity to an integer. Therefore, the IF ambiguity-fixed resolution of the PPP is available.

Experiments and analysis

In this section, 11 IGS stations evenly distributed worldwide are used for experiments, shown in Fig. 8. First, the OSR fitting accuracy with different fixed sample numbers is analyzed. Second, the positioning performance of BDS-3 GSMC-based PPP-AR is evaluated. Beyond that, the transmission performance of BDS SMC is analyzed.

OSR fitting strategy analysis

We use the latest OSR value as a_0^{OSR}. To determine the optimal sampling number for a_1^{OSR} fitting, in this section, IGS station coordinates and SSR corrections from CNES are used to fit a_1^{OSR} with different sample numbers. To evaluate the fitting precision, we set the calculated OSR on every epoch to the true value, and SSR corrections of 7 days are collected from DOY 156 to DOY 162 in 2022.

To validate the optimal fitting strategies for a_1^{OSR}, 2 to 36 samples are used to fit the parameter. Afterward, it is used to extrapolate the OSR. The extrapolation time is set from 1 to 5 min. Figure 9 shows that with the increase in the number of samples, the extrapolation error of a_1^{OSR} decreases. When the number of fitting samples reaches 36, the 5-min extrapolation error of Galileo exhibits the best accuracy, as the error is less than 0.05 m, and the values are 0.1 m and 0.18 m for GPS and BDS, respectively. Therefore, the sample numbers to fit a_1^{OSR} is set to 36, and the latest OSR value is set as a_0^{OSR} at the server.

BDS-3 GSMC PPP-AR performance analysis

To evaluate the positioning performance of real-time PPP-AR using BDS-3 GSMC (SMC-based PPP-AR), observation data from 11 IGS stations from DOY 192 to DOY 198 in 2022 are used for the experiment. The station coordinates are obtained from the solution independent exchange format (SINEX) file provided by the IGS and considered the true value while calculating the root-mean-square error (RMSE).

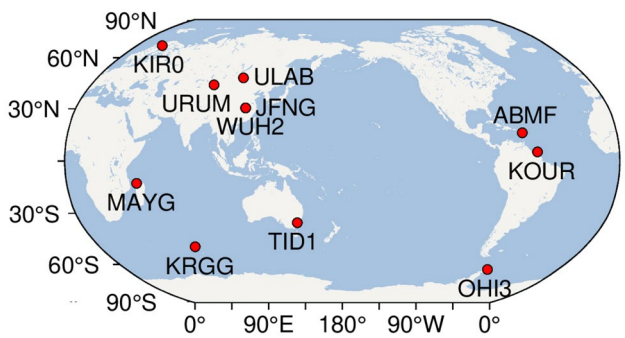

Fig. 8 Distributions of 11 IGS stations

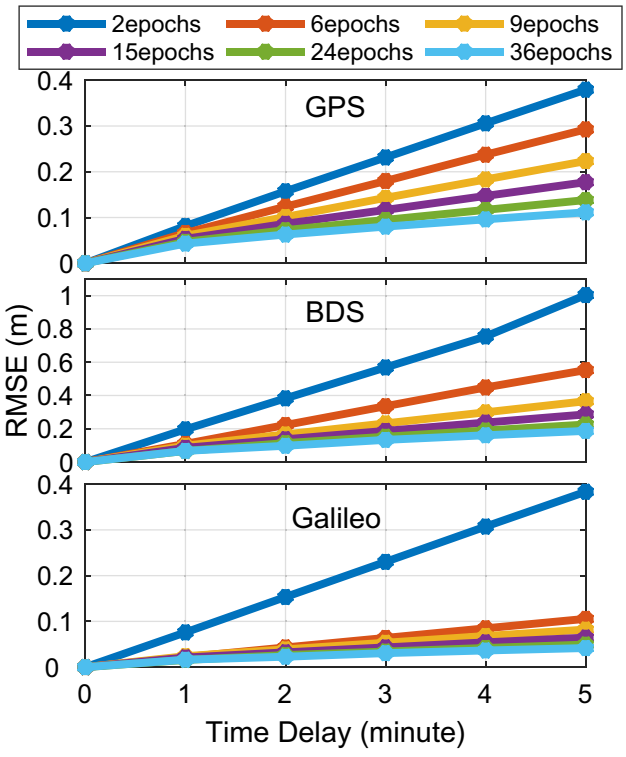

Fig. 9 Extrapolation accuracy of a_1^{OSR} with different numbers of samples for GPS, Galileo and BDS

The SMC-based PPP-AR is compared with both SMC-based PPP and PPP-AR using the original SSR corrections (SSR-based PPP-AR). Only the OSR polynomial coefficients are applied to the float-ambiguity PPP for the SMC-based PPP strategy, while the UPD corrections are unused. The performance of SMC-based PPP, SMC-based PPP-AR and SSR-based PPP-AR are assessed in terms of convergence time and positioning accuracy. In addition, the fixing rate and time to first fix (TTFF) are set as references to evaluate the PPP-AR performance.

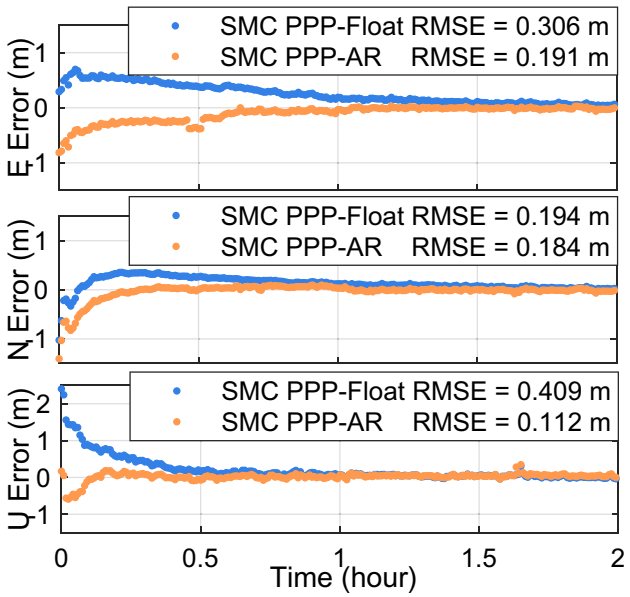

Fig. 10 Time series of the positioning error in each direction in NEU coordinates and the RMSE values. The results for SMC-based PPP-AR and SMC-based PPP are compared. Station: KRGG, DOY 192 (2022)

In this research, both static and kinematic modes are considered. The sampling interval of positioning is set as 30 s. The threshold of convergence time is set to 0.2 m for each direction in the north, east and up coordinate system (NEU) for kinematic and 0.15 m for static over 5 min. For ambiguity, GPS and Galileo satellites are fixed to integers, while BDS satellites are not involved due to the relatively poor precision of orbits and clocks. The TTFF, for both static and kinematic modes, is defined as the time when three continuous successfully fixed epochs emerge. Considering the extrapolation error and UPD time-varying error, the validity time of corrections is set to 5 min.

To compare the kinematic positioning performance of SMC-based PPP-AR and SMC-based PPP in the early period of positioning, the time series of the positioning error for the first two hours and their RMSE values are shown in Fig. 10. Compared to the SMC-based PPP, the SMC-based PPP-AR has a faster convergence time and better accuracy performance, especially in the east and up directions. Furthermore, all station statistical results for the first two hours are shown in Fig. 11. The accuracy of SMC-based PPP-AR in the horizontal and vertical directions improves by 1 cm and 12 cm on average, respectively. Compared with the SMC-based PPP, the converged station percentage is improved by 26% on average in the first 40 min.

Figure 12 shows each station's three-dimensional RMSE and convergence time of three different positioning strategies in both kinematic and static modes. For most stations, the SMC-based PPP-AR mode has better accuracy and

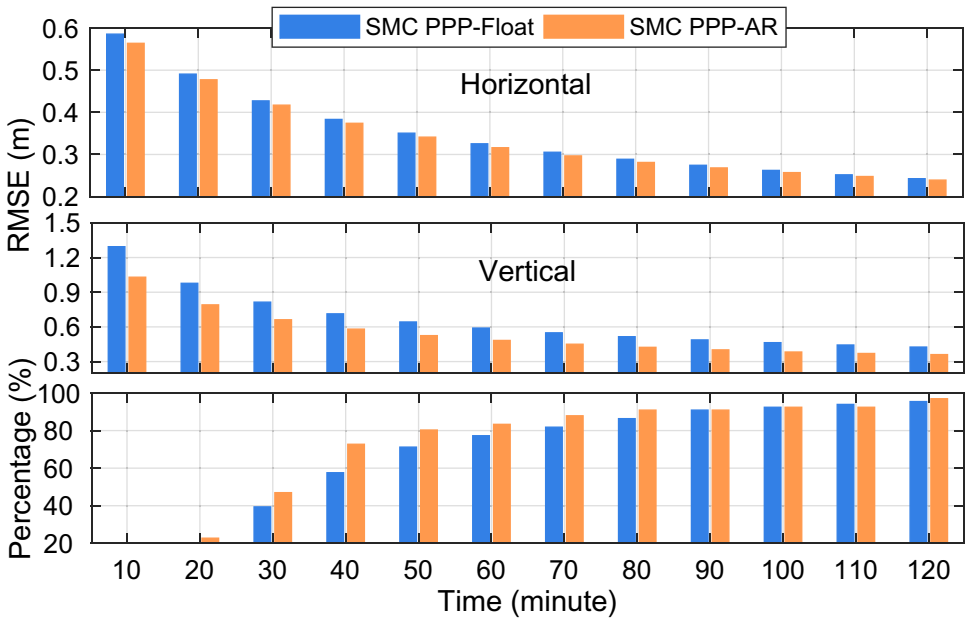

Fig. 11 Statistical results comparison between SMC-based PPP-AR and SMC-based PPP, including the horizontal RMSE (top), vertical RMSE (middle) and converged station percentage (bottom) every 10 min in the first two hours

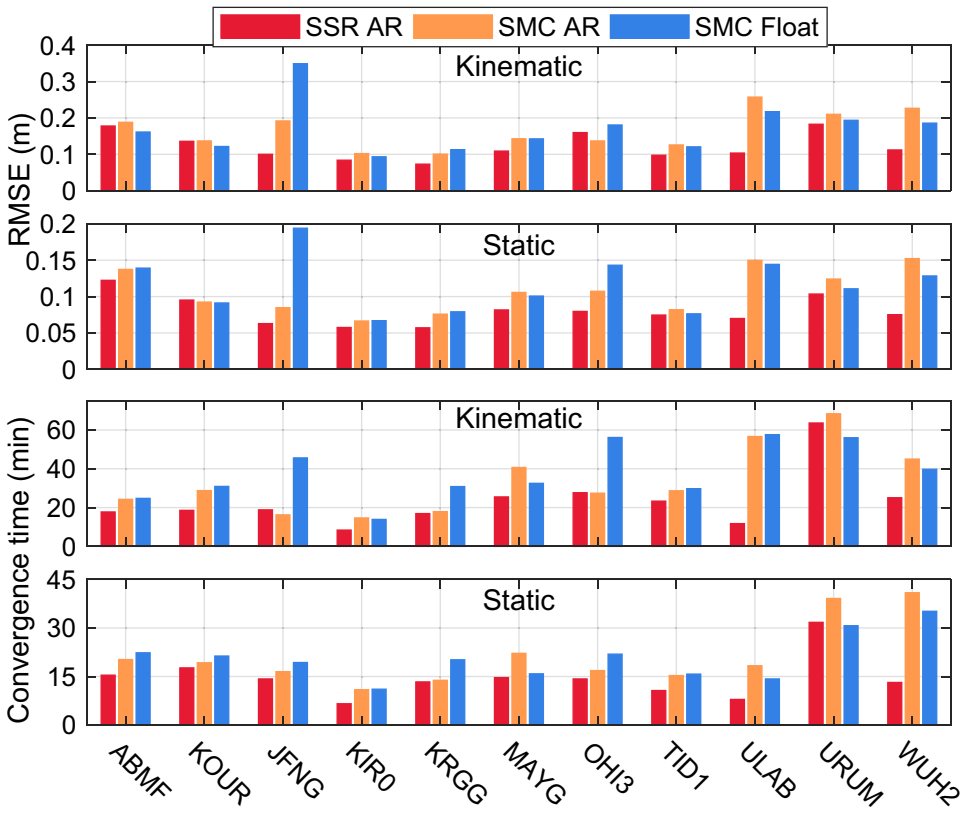

Fig. 12 Three-dimensional RMSE and convergence time at each station. Both kinematic and static results of the three different positioning modes (SMC-based PPP-AR, SMC-based PPP and SSR-based PPP-AR) are compared

Table 3 Average RMSE and convergence time for the three different strategies (SMC-based PPP-AR, SMC-based PPP and SSR-based PPP-AR)

Mode	Kinematic		Static	
	RMSE (m)	Convergence time (min)	RMSE (m)	Convergence time (min)
SSR PPP-AR	0.12	23.4	0.08	14.5
SMC PPP-AR	0.15	32.5	0.11	18.7
SMC PPP	0.17	38.0	0.12	21.2

convergence time performance than the SMC-based PPP, especially in kinematic mode. The average RMSE and convergence time are shown in Table 3. Note that the RMSE is calculated from the first epoch to the last. Thus, compared with the accuracy after convergence results (Geng et al. 2022), the RMSE values are relatively larger. Nevertheless, compared to the SMC-based PPP, the positioning accuracy of SMC-based PPP-AR improved by 10.0% and 7.8% for kinematic and static modes, respectively, and the convergence time decreased by 14.5% and 11.8% for kinematic and static modes, respectively.

Figure 13 shows the successfully fixed rate, along with the TTFF, for both SSR-based PPP-AR and SMC-based PPP-AR at each station, and the statistical results are shown in Table 4. Tables 3 and 4 show that the performance of SMC-based PPP-AR is worse than that of SSR-based PPP-AR. This is attributed to the loss of precision and reduced number of satellites while encoding, along with the OSR extrapolation error and the UPD error not being up to date.

We implement an additional experiment to further evaluate the performance of the proposed extrapolatable parameters. We manually terminate the OSR correction broadcasting in the experiment when user positioning has converged. Thereafter, PPP-AR at the user end performs with the last-received correction for 10 more minutes. Two different strategies are applied and compared. In strategy one, the a_0^{OSR} and a_1^{OSR} of the last-received epoch are extrapolated to the current epoch. In strategy two, the last-received a_0^{OSR} is used throughout the 10 min following the broadcasting strategy in Geng et al. (2022) and Gu et al. (2022), where the corrections are unable to be extrapolated. Note that in both strategies, the last-received UPDs are used to fix the ambiguity. The statistical performance is shown in Fig. 14. It can be verified that with the linear coefficients used for OSR correction prediction, centimeter accuracy is achieved until the extrapolation time reaches 7.5 min, on average. In contrast, the time is below 2.5 min without extrapolation.

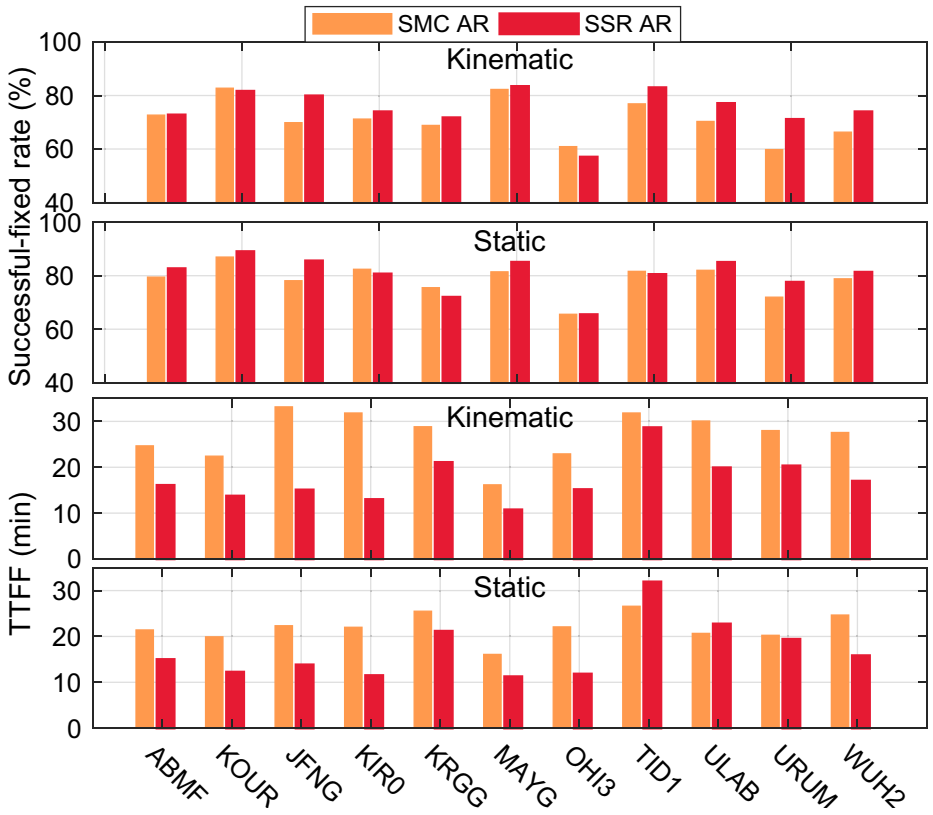

Fig. 13 Successfully fixed rate and TTFF statistics comparison for each station. Both kinematic and static results of two different ambiguity resolution modes (SMC-based PPP-AR and SSR-based PPP-AR) are compared

Table 4 Statistical results of the average successfully fixed rate and TTFF for all stations

Mode	Kinematic		Static	
	Successfully fixed rate (%)	TTFF (min)	Successfully fixed rate (%)	TTFF (min)
SSR PPP-AR	75.1	17.3	80.5	16.7
SMC PPP-AR	71.1	27.0	78.5	22.0

SMC transmission performance evaluation

In practical application situations, data loss and transmission error occur during BDS SMC signal transmission. This section uses the BDS SMC transmission host to send and receive the corrections. The BDS SMC device is shown in Fig. 15, which is provided by the China Top Communication Company. The frequency is set to 1 min, and the received message is compared with the original message generated by the server. The performance of the SMC transmission is evaluated using the transmission loss rate and error rate.

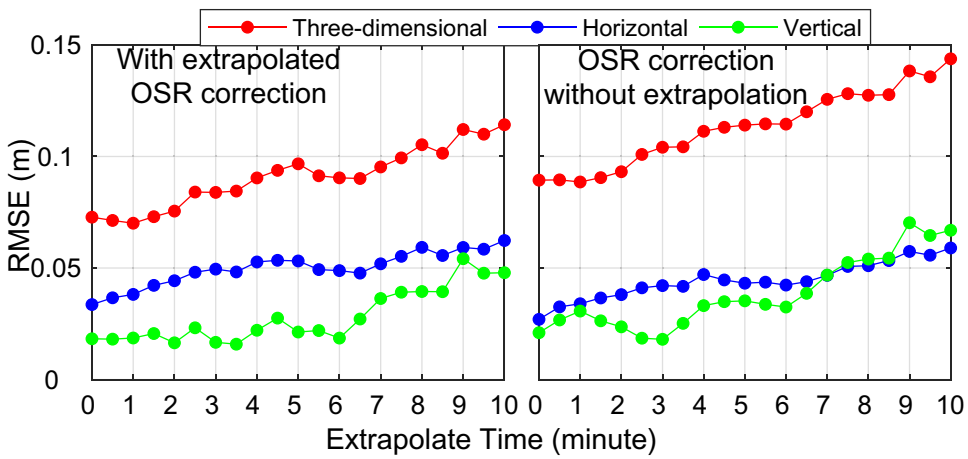

Fig. 14 Positioning accuracies with extrapolation time from 0 to 10 min. One uses a_0^{OSR} and a_1^{OSR} to extrapolate OSR correction (left), and the other uses the last-received a_0^{OSR} without extrapolation (right)

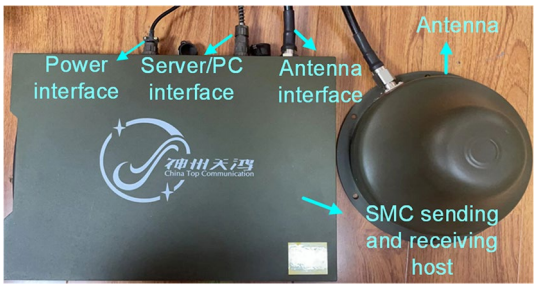

Fig. 15 BDS short-message communication device

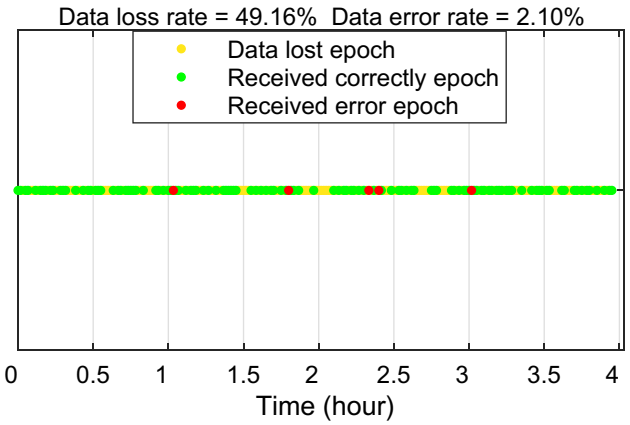

Fig. 16 Data receiving state in each epoch with the BDS SMC device

Figure 16 shows the data receiving state for each epoch with BDS SMC equipment over approximately 4 h. Compared with the original corrections, the data loss rate is more than 49%, and the data transmission error rate is approximately 2%, which may be attributed to the overload request for SMC and signal capture failure of the SMC device. The percentage of different data continuous loss durations was calculated and is shown in Table 5. Approximately 80% of the consequent data loss is no more than 2 epochs, and only 3% of the data are consecutively missed for more than 5 min; thus, the extrapolatable corrections proposed in this research can be used to develop the missing epochs.

Using the corrections received by the SMC host, PPP-AR performance is further evaluated compared to the performance with complete and correct corrections. The validity time of corrections in this experiment is set to 7.5 min. As shown in Fig. 17, attributed to missing data, the accuracy is decreased by approximately 0.9 cm and 3.0 cm in the horizontal and vertical directions, respectively. Meanwhile, the successfully fixed rate drops from 83.8% to 73.2%. Nevertheless, due to the extrapolatable parameters proposed in this research, the consecutive positioning service is achieved without interruption, although the user terminal receives only 48.7% of corrections correctly.

Conclusions

To improve global precise positioning performance using BDS-3 GSMC, we present a complete process flow for conducting real-time multi-GNSS PPP-AR using BDS-3 GSMC. Some findings from this research are summarized as follows:

(1) The short-term change trend of OSR corrections is linear, as it indicates the linear change of satellite orbit and clock errors in line of sight. Therefore, a linear fitting model is used for OSR corrections, and users may easily extrapolate the corrections using coefficients. The jump of the OSR value occurs when a broadcast ephemeris switch occurs, and for BDS in particular with CNES products, the overall jump of all satellites occurs at uncertain times. Therefore, some extra OSR correction conversions are needed for fitting. In our study, broadcasting the latest OSR as the constant and using multiple epochs to fit the linear term shows optical performance. Besides, Galileo has the best extrapolate accuracy than GPS and BDS.

(2) The correction range contributions for GPS and Galileo are relatively close together. For BDS, the correction distribution is dispersed due to the different clock datum between broadcast ephemeris and SSR corrections, along with the poor accuracy of orbit and clocks. The datum bias of BDS can be eliminated using the TGD products in the broadcast ephemeris, and the OSR range can be compressed efficiently.

(3) The priority of SMC-based PPP-AR is more obvious in the early period of positioning, as the vertical accuracy improved by 12 cm on average for the first two hours compared with SMC-based PPP-float method. As the full-day statistical results indicate, the SMC-based PPP-AR performs better in terms of both convergence time and accuracy, improved by 14.5% and 10.0% for kinematic mode and 7.8% and 11.8% for kinematic mode for static mode, respectively. Moreover, when GSMC interruption occurs, the extrapolatable param-

Table 5 Continuous data loss duration

Consecutive missing data time (minutes)	1	2	3	4	5	> 5
Percentage (%)	58.5	20.0	9.2	4.6	4.6	3.0

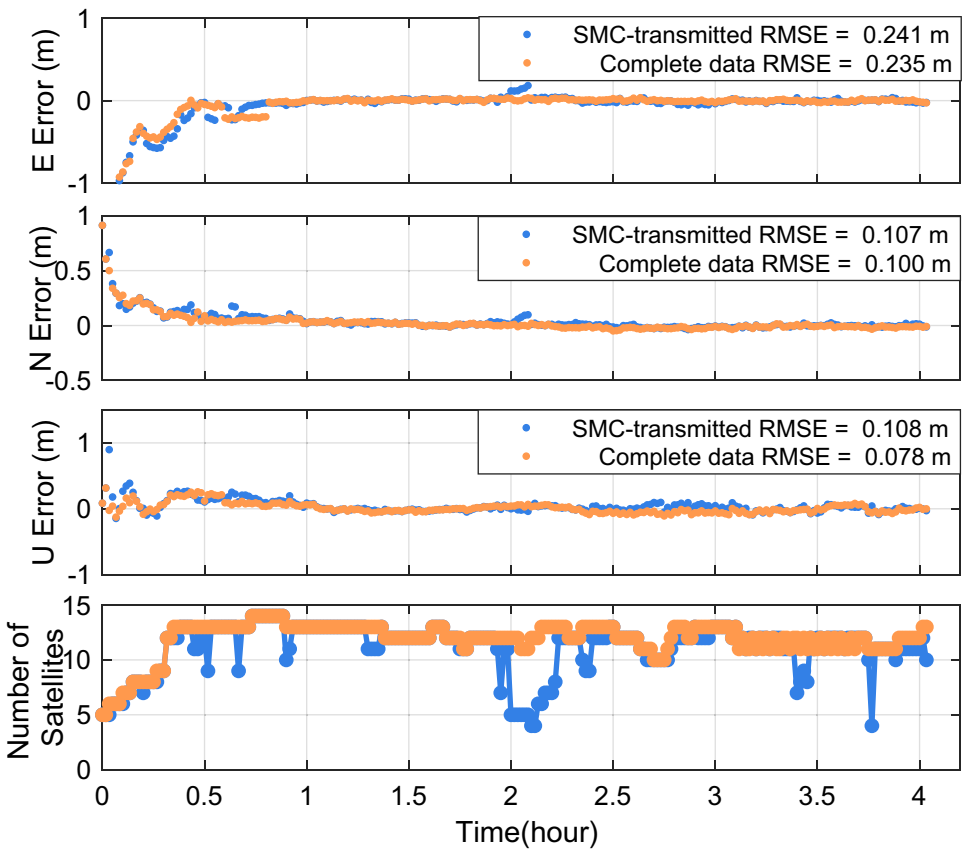

Fig. 17 Error time series and RMSE values in each direction in NEU coordinates (top three), along with the number of satellites (bottom) using SMC-transmitted corrections compared with those using complete corrections. Station: KOUR, DOY 192 (2022)

eters can effectively suppress the accuracy loss and prolong the validity time of corrections.

(4) Missing short-term data and errors occur often when using the BDS SMC for correction transmission. Nonetheless, the results show that the negative influence of missing short-term data and error is significantly reduced when the coefficients are used to predict the OSR corrections.

It should be pointed out that since we use the UPD method for ambiguity resolution, high-quality observation data are required for wide-lane ambiguity fixing. Therefore, the successfully fixed rate may be significantly reduced when processing real-time kinematic observation data with large noise and multipath effects. The above will be further studied.

Acknowledgements The GNSS data provided by the IGS Multi-GNSS Experiment (MGEX) network and real-time SSR corrections provided by CNES are appreciated. This research is supported by the Program of Shanghai Academic Research Leader; the National Key R&D Program of China (No. 2018YFB0504300); Key R&D Program of Guangdong Province (No. 2018B030325001); the National Natural Science Foundation of China (No. 11673050); and the Key Program of Special Development funds of Zhangjiang National Innovation Demonstration Zone (Grant No. ZJ2018-ZD-009).

Author contributions In this paper, JC, ZS and YZ were responsible for algorithm design. YZ and ZS were responsible for the experiments and analysis. CY and ZS were responsible for the device test. ZS drafted the paper writing. JD optimized the picture format and layout in the paper. All authors have read and agreed to the published version of the manuscript.

Funding This research is supported by the Program of Shanghai Academic Research Leader (No. 20XD1404500); the National Key R&D Program of China (No. 2018YFB0504300); Key R&D Program of Guangdong province (No. 2018B030325001); the National Natural Science Foundation of China (No. 11673050); and the Key Program of Special Development funds of Zhangjiang National Innovation Demonstration Zone (Grant No. ZJ2018-ZD-009).

Data availability The GNSS data are provided by the IGS and can be achieved through ftp:// gdc.cddis.eosdis.nasa.gov. The real-time SSR corrections are provided by CNES and can be achieved through RTCM stream provided by Shanghai Astronomical Observatory, the mount point of stream is: 112.65.161.226:2101/SSRA00CNE0.

Declarations

Conflict of interest The authors declare no conflict of interest.

Ethics approval and consent to participate Not applicable for the Ethics approval. All authors approved to participate in this work.

Consent for publication All authors approved the final manuscript and the submission to the journal.

References

Chen J et al (2013) Performance of real-time precise point positioning. Mar Geodesy 36(1):98–108

Chen J, Wang A, Zhang Y, Zhou J, Yu C (2020) BDS Satellite-based augmentation service correction parameters and performance assessment. Remote Sens 12(5):766–784

Chen C, Xiao G, Chang G, Xu T, Yang L (2021) Assessment of GPS/Galileo/BDS precise point positioning with ambiguity resolution using products from different analysis centers. Remote Sens 13(16):3266–3285

Chen J, Zhang Y, Yu C, Ding J (2022a) Processing algorithms and performance evaluation of BDS RDSS location reporting service. Acta Geod Et Cartogr 51(4):511–521

Chen J, Wang J, Yu C, Zhang Y, Wang B (2022b) Improving BDS broadcast ephemeris accuracy using ground-satellite-link observations. Sat Nav 3(11):1–12

Chen J, Zhang Y, Wang A, Yu C, Song Z, Zhou J (2022c) Models and performance of SBAS and PPP of BDS. Sat Nav 3(11):1–12

CSNO (2015) Performance requirements and test methods for BDS RDSS unit. Chinese Satellite Navigation Office (CSNO), Beijing, China

CSNO (2019) Development of the BeiDou navigation satellite system, version 4.0. China Satellite Navigation Office (CSNO), Beijing, China

CSNO (2021) BeiDou navigation satellite system open service performance standard (Version 3.0). Chinese Satellite Navigation Office (CSNO), Beijing, China

Ge M, Gendt G, Rothacher M (2008) Resolution of GPS carrier-phase ambiguities in precise point positioning (PPP) with daily observations. J Geod 82(7):389–399

Geng J, Meng X, Dodson A, Teferle F (2010) Integer ambiguity resolution in precise point positioning: method comparison. J Geod 84(9):569–581

Geng J, Shi C, Ge M, Dodson A, Lou Y, Zhao Q (2012) Improving the estimation of fractional-cycle biases for ambiguity resolution in precise point positioning. J Geod 86(8):579–589

Geng J, Yang S, Guo J (2021) Assessing IGS GPS/Galileo/BDS-2/BDS-3 phase bias products with PRIDE PPP-AR. Sat Nav 2(17):1–15

Geng T, Ma Z, Xie X, Tao J, Liu T, Zhao Q, Li J (2022) Multi-GNSS real-time precise point positioning using BDS-3 global-short message communication to broadcast corrections. GPS Solut 26(99):1–13

Gu S, Guo R, Gong X, Zhang S, Lou Y, Li Z (2022) Real-time precise point positioning based on BDS-3 global short message communication. GPS Solut 26(107):1–14

IGS (2020) IGS state space representation (SSR) format version 1.00. RTCM SC-104 SSR working group and IGS real-time working group, Arlington, TX, USA. Avaliable on https://files.igs.org/pub/data/format/

Kouba J, Héroux P (2001) Precise point positioning using IGS orbit and clock products. GPS Solut 5(2):12–28

Li B, Verhagen S, Teunissen P (2013) GNSS integer ambiguity estimation and evaluation: LAMBDA and Ps-LAMBDA. Lect Notes Electr Eng 244(1):291–301

Li B, Zhang Z, Zang N, Wang S (2019) High-precision GNSS ocean positioning with BeiDou short-message communication. J Geod 93:125–139

Li G, Guo S, Lv J, Zhao K, He z (2021) Introduction to global short message communication service of BeiDou-3 navigation satellite system. Adv Space Res 67(5):1701–1708

Li B, Ge H, Bu Y, Zheng Y, Yuan L (2022) Comprehensive assessment of real-time precise products from IGS analysis centers. Sat Nav 3(12):1–17

Liu T, Jiang W, Laurichesse D, Chen H, Liu H, Wang J (2020) Assessing GPS/Galileo real-time precise point positioning with ambiguity resolution based on phase biases from CNES. Adv Space Res 66(4):810–825

Malys S, Jensen PA (1990) Geodetic point positioning with GPS carrier beat phase data from the CASA UNO experiment. Geophys Res Lett 17(5):651–654

Nie Z, Wang B, Wang Z, He K (2020) An offshore real-time precise point positioning technique based on a single set of BeiDou short-message communication devices. J Geod 94(9):1–11

RTCM Special Committee (2016) RTCM standard 10403.3 differential GNSS (Global Navigation Satellite Systems) services-version 3. RTCM Special Committee No. 104, Arlington, TX, USA

Shi J, Yuan X, Cai Y, Wang J (2017) GPS real-time precise point positioning for aerial triangulation. GPS Solut 21(2):405–414

Teunissen P (1995) The least-squares ambiguity decorrelation adjustment: A method for fast GPS integer ambiguity estimation. J Geod 70(1–2):65–82

Wang A, Zhang Y, Chen J, Wang H (2022) Improving the (re-)convergence of multi-GNSS real-time precise point positioning through regional between-satellite single-differenced ionospheric augmentation. GPS Solut 26(2):26–39

Weber G, Mervart L, Lukes Z, Rocken C, Dousa J (2007) Real-time clock and orbit corrections for improved point positioning via NTRIP. In: Proceedings of ION GNSS 2007, Fort Worth, Texas, USA, pp 1992–1998

Yang Y, Gao W, Guo S, Mao Y, Yang Y (2019) Introduction to BeiDou-3 navigation satellite system. Navigation 66(1):7–18

Zhang Y, Kubo N, Chen J, Chu F, Wang A, Wang J (2020) Apparent clock and TGD biases between BDS-2 and BDS-3. GPS Solut 24(1):1521–1886

Zumberge JF, Heflin MB, Jefferson DC, Watkins MM, Webb FH (1997) Precise point positioning for the efficient and robust analysis of GPS data from large networks. J Geophys Res Solid Earth 102(B3):5005–5017

Ziyuan Song is a Ph.D. student at Shanghai Astronomical Observatory (SHAO), Chinese Academy of Sciences (CAS). He obtained his bachelor's degree in 2018 from Shandong University of Science and Technology, China. His current research is on GNSS satellite and ground-based augmentation systems and Multi-GNSS precise point positioning with ambiguity resolution.

Junping Chen is a professor and the head of the GNSS data analysis group at Shanghai Astronomical Observatory (SHAO), Chinese Academy of Sciences (CAS). He received his Ph.D. degree in Satellite Geodesy from Tongji University in 2007. He worked as a research scientist at the GFZ German Research Centre for Geosciences from 2006 to 2011. Since 2011, he has been supported by the "one hundred talents" program of the Chinese Academy of Sciences. His research interests include multi-GNSS data analysis and GNSS augmentation systems.

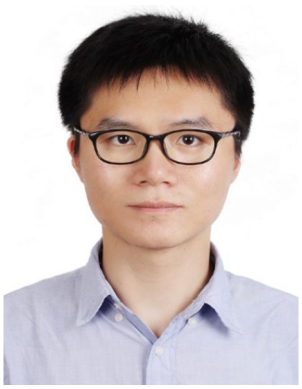

Yize Zhang is currently an associate professor at Shanghai Astronomical Observatory (SHAO), Chinese Academy of Sciences (CAS). He received his Ph.D. degree from Tongji University in 2017. Then, he did his postdoctoral research at the Tokyo University of Marine Science and Technology (TUMSAT). His current research mainly focuses on multi-GNSS precise positioning and GNSS biases analysis.

Chao Yu is a Ph.D. student at Shanghai Astronomical Observatory (SHAO), Chinese Academy of Sciences (CAS). He obtained his bachelor's degree in 2017 from Chang'an University, China. His current research is on precise orbit determination of low-orbit satellites, GNSS precise positioning and data analysis.

Junsheng Ding is a Ph.D. student at Shanghai Astronomical Observatory (SHAO), Chinese Academy of Sciences (CAS). He obtained his bachelor's degree in 2018 from Chang'an University, China. His current research is on GNSS high-precision positioning with satellite augmentation, GNSS meteorology and PPP-RTK atmosphere modeling.